

## Experimental Observation of Spin-Exchange in Ultracold Fermi Gases \*

Peng Peng(彭鹏)<sup>1,2</sup>, Liang-Hui Huang(黄良辉)<sup>1,2\*\*</sup>, Dong-Hao Li(李东豪)<sup>1,2</sup>, Zeng-Ming Meng(孟增明)<sup>1,2</sup>,  
Peng-Jun Wang(王鹏军)<sup>1,2</sup>, Jing Zhang(张靖)<sup>1\*\*</sup>

<sup>1</sup>State Key Laboratory of Quantum Optics and Quantum Optics Devices, Institute of Opto-electronics,  
Shanxi University, Taiyuan 030006

<sup>2</sup>Collaborative Innovation Center of Extreme Optics, Shanxi University, Taiyuan 030006

(Received 6 November 2017)

We experimentally study the spin exchange collision in ultracold <sup>40</sup>K Fermi gases. The quadratic Zeeman shift, trap potential and temperature of atomic cloud will influence on the spin changing dynamics. Dependences of the spin components populations on the external bias magnetic field, the optical trap depth and the temperature of atomic cloud are experimentally investigated. The spin exchange from the initial states to the final state are observed for different initial states. This work shows an interesting process of reaching equilibrium by redistribution among the spin states with the spin exchange collision in an ultracold large-spin Fermi gas.

PACS: 34.20.Cf, 67.85.Hj, 03.75.Lm

DOI: 10.1088/0256-307X/35/3/033401

Ultracold atomic gases provide an exceptional experimental platform to mimic numerous interesting phenomena in high energy physics and condensed matter,<sup>[1]</sup> in which nearly perfect isolation from environmental influences and the physical parameters in experiment can be precisely controlled, including the atomic number, the ultracold-sample temperature, the shape of external trapping potential, the strength of the atom-atom interaction, and the dimensionality of the system.<sup>[2–4]</sup> Especially, cold and ultracold atomic collisions<sup>[5]</sup> occupy a strategic position in quantum simulation of chemical physics, condensed matter physics. The nature of these collisions has a critical bearing on the precision measurement of molecular and atomic properties, matter-wave coherence and quantum-statistical condensates, and optical manipulation of inelastic and reactive processes.<sup>[5]</sup>

Since BEC was successfully prepared in experiment, many groups have experimentally investigated spin collisions in BEC, such as spin exchange among different spin states, transition energy of spin exchange, which provides an approach for generating spin squeezing and entangled states for precision measurements.<sup>[6–11]</sup> Recently, the coherent spin population oscillations was also observed in a thermal Bose gas of <sup>23</sup>Na.<sup>[12]</sup> Manipulating spin exchange interaction can simulate classic and quantum magnetism in an optical lattice potential.<sup>[13–15]</sup>

In contrast, fermions are governed by the Pauli blocking and reveal a different behavior. Research of spin exchange in Fermi gases is less than that in Bose gases. The first coherent spin dynamics (i.e., spin oscillations) induced by the spin exchange interaction of <sup>40</sup>K atoms was observed in a deep optical lattice.<sup>[16]</sup> Later, the giant spin oscillation of a Fermi sea in the many-body case was also found in a harmonic trap.<sup>[17]</sup>

Most recently, the spin relaxation mechanism was systematically checked.<sup>[18]</sup> Moreover, fermionic high-spin systems with more than two spin components constitute a completely new class of many-body systems.<sup>[19]</sup> In this study, we present the experimental realization of spin exchange in ultracold Fermi gases by tuning the external magnetic field and depth of the optical dipole trap. Here the spin relaxation is studied in a harmonic optical trap. Moreover, we give more detailed studies for the spin relaxation and consider more factors, such as trap potential depth, and different initial spin mixture states, which is different from Ref. [18].

We consider a simple model with four energy levels as shown in Fig. 1(a), choosing  $|1/2 \oplus -1/2\rangle$  ( $|F = 9/2, m_F = 1/2\rangle$  and  $|F = 9/2, m_F = -1/2\rangle$ ) and  $|3/2 \oplus -3/2\rangle$  as the initial and final states, relatively. The energy of  $|1/2 \oplus -1/2\rangle$  becomes lower than that of  $|3/2 \oplus -3/2\rangle$  with the increasing bias magnetic field, as shown in Fig. 1(b). To understand collective spin changing dynamics, we first consider the underlying microscopic collisions, well described by s-wave scattering in a simple case. Here the two fermionic atoms collide and change their spin configuration ( $m_{F_1}, m_{F_2} \rightarrow m_{F_3}, m_{F_4}$ ), conserving the total magnetization ( $m_{F_1} + m_{F_2} = m_{F_3} + m_{F_4}$ ) and obeying the Pauli exclusion principle ( $m_{F_1} \neq m_{F_2}$  and  $m_{F_3} \neq m_{F_4}$ ).<sup>[17]</sup> The interplay between different quadratic Zeeman energies and differential spin dependent interaction energies determines whether spin exchange can occur or not.<sup>[3]</sup> Moreover, since fermions have the Fermi energy in the trap due to Pauli blocking, spin exchange from  $|1/2 \oplus -1/2\rangle$  to  $|3/2 \oplus -3/2\rangle$  can occur even at higher magnetic field as shown in Fig. 1(a) although the energy of  $|3/2 \oplus -3/2\rangle$  is higher than that of  $|1/2 \oplus -1/2\rangle$ . For <sup>40</sup>K atoms in the  $F = 9/2$  manifold, the prepared  $|1/2 \oplus -1/2\rangle$  can

\*Supported by the National Key Research and Development Program of China under Grant Nos 2016YFA0301600 and 2016YFA0301602, the National Natural Science Foundation of China under Grant Nos 11234008, 11474188, and 11704234, and the Fund for Shanxi '1331 Project' Key Subjects Construction.

\*\*Corresponding author. Email: huanglh06@126.com; jzhang74@sxu.edu.cn

© 2018 Chinese Physical Society and IOP Publishing Ltd

be spin exchanged into other states  $|5/2 \oplus -5/2\rangle$ ,  $|7/2 \oplus -7/2\rangle$  and  $|9/2 \oplus -9/2\rangle$ .

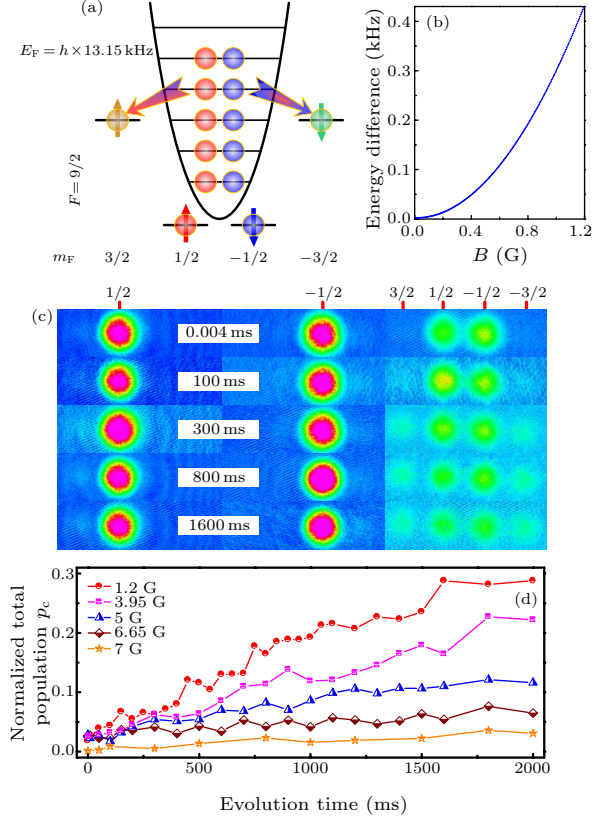


**Fig. 1.** (Color online) Spin-exchange in ultracold Fermi gases. (a) Schematic of a spin mixing process between  $|1/2 \oplus -1/2\rangle$  and  $|3/2 \oplus -3/2\rangle$ . (b) Energy difference between  $|3/2 \oplus -3/2\rangle$  and  $|1/2 \oplus -1/2\rangle$  as the function of the external magnetic field. (c) TOF image in  $|1/2 \oplus -1/2\rangle$  and  $|3/2 \oplus -3/2\rangle$  states. The left, middle and right panels are the atomic population with different evolution times when the initial states are only  $|F = 9/2, m_F = 1/2\rangle$ ,  $|F = 9/2, m_F = -1/2\rangle$ , and  $|1/2 \oplus -1/2\rangle$ , respectively. Here the external magnetic field is 1.2 G. (d) Normalized populations in spin states  $|3/2 \oplus -3/2\rangle$  as a function of evolution time at external magnetic field with 1.2, 3.95, 5, 6.65 and 7 G, respectively.

The fermionic gas of  $^{40}\text{K}$  atoms in the  $F = 9/2$  manifold is employed in experiment. We sympathetically cool spin polarized  $^{40}\text{K}$  atoms in the spin state  $|F = 9/2, m_F = 9/2\rangle$  with the  $^{87}\text{Rb}$  atoms at the spin state  $|F = 2, m_F = 2\rangle$  to  $1.5 \mu\text{K}$  by radio-frequency evaporation cooling in the quadrupole-Ioffe configuration (QUIC) trap, and then transport them into the center of the glass cell in favor of optical access, which is used in previous experiments,<sup>[20–23]</sup> where  $F$  denotes the total spin, and  $m_F$  is the magnetic quantum number. Subsequently, we transfer the atoms into the optical dipole trap, and typically obtain the degenerate Fermi gas of ( $\sim 4 \times 10^6$ )  $^{40}\text{K}$  atoms in the lowest hyperfine Zeeman state  $|F = 9/2, m_F = 9/2\rangle$  by gradually decreasing the depth of the optical trap. Finally, we obtain ultracold Fermi gases with the temperature about  $0.3T_F$ , where the Fermi temperature is defined by  $T_F = \hbar\bar{\omega}(6N)^{1/3}/k_B$  with  $\bar{\omega} = (\omega_x\omega_y\omega_z)^{1/3} \simeq$

$2\pi \times 80 \text{ Hz}$  being the geometric mean of the optical trap frequency for  $^{40}\text{K}$  degenerate Fermi gas in our experiment,  $N$  the particle number of  $^{40}\text{K}$  atoms, and  $k_B$  the Boltzmann constant. We use a resonant laser beam pulse (780 nm) for 0.03 ms to remove the  $^{87}\text{Rb}$  atoms in the mixture without losing and heating  $^{40}\text{K}$  atoms. A homogeneous magnetic bias field  $B_{\text{exp}}$  is applied in the  $z$  axis (gravity direction) by a pair of quadrupole coils described in Ref. [24], which generates a Zeeman splitting  $\hbar\omega_Z = g\mu_B B_{\text{exp}}$  between two magnetic sub-levels.

To prepare different spin mixtures, the atoms of the  $|F = 9/2, m_F = 9/2\rangle$  state in optical dipole trap are firstly transferred into the lowest state  $|F = 9/2, m_F = 1/2\rangle$  in a rapid adiabatic passage induced by an rf field with a duration of 80 ms at  $B \simeq 19.6 \text{ G}$ , where the center frequency of the rf field is 6.42 MHz and the scanning width is 0.28 MHz. Then, we prepare the ultracold Fermi gases in a binary spin mixture of  $|1/2 \oplus -1/2\rangle$  with a  $\pi/2$  pulse of rf field still at 19.6 G. Subsequently, we quench the magnetic field to an expected field with a value  $B_{\text{exp}}$  during 1 ms to observe the process of spin exchange collisions with the time evolution. According to two physical restrictions, the prepared  $|1/2 \oplus -1/2\rangle$  can be coupled to other states  $|3/2 \oplus -3/2\rangle$ ,  $|5/2 \oplus -5/2\rangle$ ,  $|7/2 \oplus -7/2\rangle$  and  $|9/2 \oplus -9/2\rangle$ . We even can observe the spin exchange in the  $|7/2 \oplus -7/2\rangle$  and  $|9/2 \oplus -9/2\rangle$  state when the external magnetic field  $B_{\text{exp}}$  is lower enough. Lastly, we immediately turn off the optical trap, and the magnetic field, let the atoms ballistically expand in 12 ms and take the time-of-flight (TOF) absorption image. For the final stage, we apply a magnetic field gradient in the first 10 ms during free expansion, which creates a spatial separation of different Zeeman states due to the Stern–Gerlach effect. Then the number of atoms from  $|9/2, 9/2\rangle$  to  $|9/2, -9/2\rangle$  are measured through the TOF image, as shown in Fig. 1(c).

To make sure that the spin relaxation is not induced by the effect of magnetic field fluctuation, we prepare the single spin (spin polarized) state and check if the spin can be flipped by the magnetic field noise with the long holding time as shown in the left of Fig. 1(c). We can see that there is no spin flip with a long holding time when the single spin state  $|F = 9/2, m_F = -1/2\rangle$  (or  $|F = 9/2, m_F = 1/2\rangle$ ) is prepared. The effect of magnetic field noise is obvious at the lower field ( $< 0.1 \text{ G}$ ) in our setup. In other words, the magnetic field noise only has this significant effect on spin flip at very low bias magnetic field. Thus we make sure that the magnetic field noise cannot induce spin relaxation in our experimental system when the magnetic field is larger than 0.1 G.

Firstly, we prepare the spin mixture in the states of  $|1/2 \oplus -1/2\rangle$ , and obtain the different evolutionary processes of spin exchange at different magnetic fields. It shows that the energy difference between  $|3/2 \oplus -3/2\rangle$  and  $|1/2 \oplus -1/2\rangle$  depends on the external magnetic field. We find that the higher the

magnetic field is, the lower the rate of spin exchange is in Figs. 1(d) and 2(a). With increasing  $B_{\text{exp}}$ , the spin exchange process in  $|9/2 \oplus -9/2\rangle$ ,  $|7/2 \oplus -7/2\rangle$ ,  $|5/2 \oplus -5/2\rangle$  and  $|3/2 \oplus -3/2\rangle$  states will vanish in the higher field as shown in Fig. 2(a). To better quantitatively describe the evolution process, we define the normalized total occupation  $p_c = N/N_t = 1 - N_0/N_t = 1 - (N_{1/2} + N_{-1/2})/N_t$ , which includes all the generated spin states by spin exchange such as  $|3/2 \oplus -3/2\rangle$ ,  $|5/2 \oplus -5/2\rangle$ ,  $|7/2 \oplus -7/2\rangle$  and  $|9/2 \oplus -9/2\rangle$ . Here  $N_{1/2}$  ( $N_{-1/2}$ ) is the atomic number in the  $|F = 9/2, m_F = 1/2\rangle$  ( $|F = 9/2, m_F = -1/2\rangle$ ) state, and  $N_t$  is the total atomic number of all spin states. We also define the normalized individual occupation  $p_i = (N_{1/2+i} + N_{-1/2-i})/N_t$ , where  $i = 1, 2, \dots$  thus  $p_c = \sum p_i$ . With the increase of the external magnetic field, the atomic number in the other eight states induced by spin exchange collision is decreasing in Fig. 1(d). As shown in Fig. 1(d), there is a very weak process of spin changing collisions at the magnetic field 7 G. In other words, the spin changing collisions are suppressed in the high magnetic field. At the very low magnetic field, the two energy scales become comparable, and resonant spin oscillations are induced.<sup>[17]</sup>

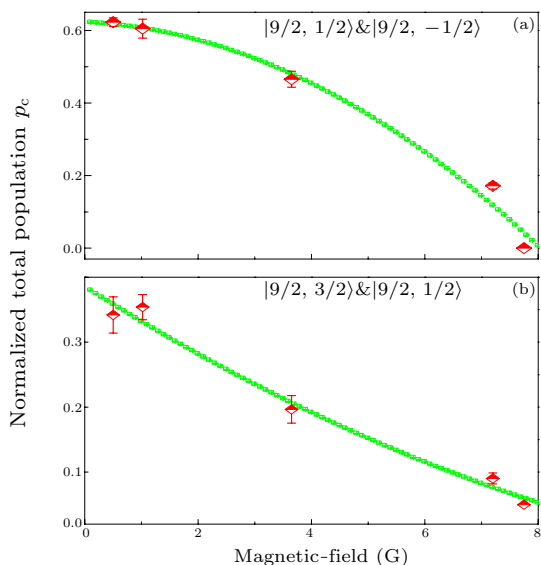


**Fig. 2.** (Color online) Dependence of spin exchange on external magnetic field. (a) The normalized spin population for the initial state  $|1/2 \oplus -1/2\rangle$  as the function of the external magnetic field. (b) The normalized spin population for the initial state  $|3/2 \oplus 1/2\rangle$  as the function of the external magnetic field. Spin populations are measured after 2000 ms. The error bars in (a) and (b) represent the standard deviation of three repeated measurements. The green symbol is the data fitting curve in the exponential function form.

Moreover, to study the spin exchange collisions in other different initial states, we prepare the state at the mixture of  $|3/2 \oplus 1/2\rangle$ . The total magnetic quantum number  $M$  in  $|3/2 \oplus 1/2\rangle$  is larger than  $|1/2 \oplus -1/2\rangle$ . The generated spin states by spin exchange for the initial state  $|3/2 \oplus 1/2\rangle$  may be

$|5/2 \oplus -1/2\rangle$ ,  $|7/2 \oplus -3/2\rangle$ , and  $|9/2 \oplus -5/2\rangle$ . We find that the spin exchange collisions for the initial state  $|3/2 \oplus 1/2\rangle$  is similar to the case of  $|1/2 \oplus -1/2\rangle$  as shown in Fig. 2(a). However, the normalized occupation  $p_c$  in initial spin mixture  $|3/2 \oplus 1/2\rangle$  is smaller than  $p_c$  in the  $|1/2 \oplus -1/2\rangle$  state.

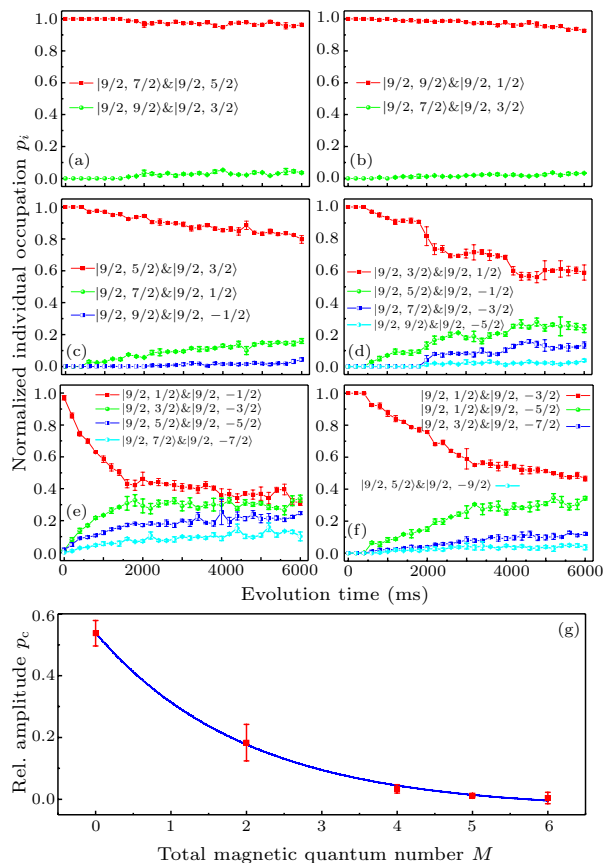


**Fig. 3.** (Color online) Spin-exchange collisions for different initial spin mixtures. (a)–(f) The normalized individual occupation  $p_i$  as a function of evolution time for the different initial spin mixture states of  $|7/2 \oplus 5/2\rangle$ ,  $|9/2 \oplus 1/2\rangle$ ,  $|5/2 \oplus 3/2\rangle$ ,  $|3/2 \oplus 1/2\rangle$ ,  $|1/2 \oplus -1/2\rangle$ , and  $| -1/2 \oplus -3/2\rangle$ . (g) The relationship between the normalized spin population of spin change collisions and the total magnetic quantum number of  $M$  ( $m_{F_1} + m_{F_2}$ ). The experimental parameters are  $B_{\text{exp}} = 0.5$  G,  $T = 0.3T_F$ , and evolution time 2000 ms. Error bars indicate the standard deviation of three repeated measurements. The green symbol is the data fitting curve in the exponential function form.

Figure 3 shows the spin exchange collisions with different spin mixtures  $|7/2 \oplus 5/2\rangle$ ,  $|9/2 \oplus 1/2\rangle$ ,  $|5/2 \oplus 3/2\rangle$ ,  $|3/2 \oplus 1/2\rangle$ ,  $|1/2 \oplus -1/2\rangle$ , and  $| -1/2 \oplus -3/2\rangle$  at a certain value of external magnetic field. The normalized individual occupation  $p_i$  as a function of evolution time for the different initial spin mixture states are measured as shown in Figs. 3(a)–3(f). The relationship between the normalized spin population of spin exchange collisions and the total magnetic quantum number  $M$  ( $m_{F_1} + m_{F_2}$ ) of the spin mixture is plotted in Fig. 3(g). These results indicate that the rate of spin exchange is inversely proportional to the total magnetic quantum number  $M$ .

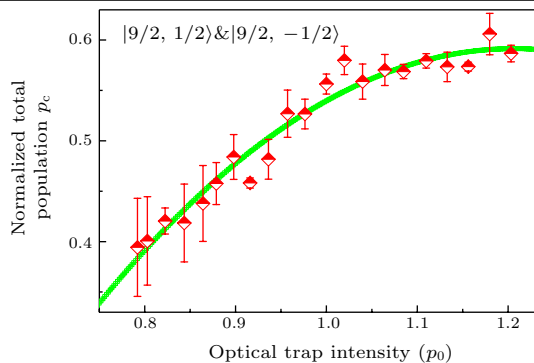


**Fig. 4.** (Color online) Dependence of spin exchange on the trap depth. Spin population is measured after the evolution time of 2000 ms. The experimental parameters are  $B_{\text{exp}} = 0.5$  G, and  $T = 0.3T_F$ . Error bars indicate the standard deviation of three repeated measurements. The green symbol is the data fitting curve in the exponential function form.

Moreover, we study the influence of the optical trap depth on spin exchange collisions. When the optical trap depth is increased by rising the power of the optical dipole trap, the Fermi energy of Fermi gases is increased, therefore the spin exchange collision is enhanced. The mixing states at  $|1/2 \oplus -1/2\rangle$  are prepared with the external magnetic field 0.5 G. The relationship between the atomic occupation in the other eight states and optical trap frequency is obtained as shown in Fig. 4. We find that the amplitude of spin exchange depends on the trap frequency. Note that we only observe the spin exchange damping instead of spin oscillation<sup>[17]</sup> since the external magnetic field is higher.

In conclusion, we have investigated the spin exchanging processes in ultracold Fermi gases with different initial spin mixtures and external magnetic fields. We study the influence of the optical trap depth on spin exchange collisions. This work will broaden the understanding of many-body spin exchanging dynamics and may lay the foundation for the future work, such as investigation of the spin squeezing in fermi gases just like in BEC.<sup>[6–11]</sup>

## References

- [1] Bloch I, Dalibard J and Zwerger W 2008 *Rev. Mod. Phys.* **80** 885
- [2] Chin C, Grimm R, Julienne P and Tiesinga E 2010 *Rev. Mod. Phys.* **82** 1225
- [3] Stamper-Kurn D M and Ueda M 2013 *Rev. Mod. Phys.* **85** 1191
- [4] Black A T, Gomez E, Turner L D, Jung S and Let P D 2007 *Phys. Rev. Lett.* **99** 070403
- [5] Weiner J, Bagnato V S, Zilio S and Julienne P S 1999 *Rev. Mod. Phys.* **71** 463
- [6] Estève J, Gross C, Weller A, Giovanazzi S and Oberthaler M K 2008 *Nature* **455** 1216
- [7] Gross C, Zibold T, Nicklas E, Estève J and Oberthaler M K 2010 *Nature* **464** 1165
- [8] Riedel M F, Böhi P, Li Y, Hänsch T W, Sinatra A and Treutlein P 2010 *Nature* **464** 1170
- [9] Gross C, Strobel H, Nicklas E, Zibold T, Bar-Gill N, Kurizki G and Oberthaler M K 2011 *Nature* **480** 219
- [10] Zhang Z and Duan L M 2013 *Phys. Rev. Lett.* **111** 180401
- [11] Luo X Y, Zou Y Q, Wu L N, Liu Q, Han M F, Tey M K and You L 2017 *Science* **355** 620
- [12] Pechkis H K, Wrubel J P, Schwettmann A, Griffin P F, Barnett R, Tiesinga E and Lett P D 2013 *Phys. Rev. Lett.* **111** 025301
- [13] Widera A, Gerbier F, Foelling S, Gericke T, Mandel O and Bloch I 2005 *Phys. Rev. Lett.* **95** 190405
- [14] Struck J, Ölschlager C, Le Targat R, Soltan-Panahi P, Eckardt A, Lewenstein M, Windpassinger P and Sengstock K 2011 *Science* **333** 996
- [15] Simon J, Bakr W S, Ma R, Eric Tai M, Preiss P M and Greiner M 2011 *Nature* **472** 307
- [16] Krauser J S, Heinze J, Fläschner N, Götze S, Jürgensen O, Lühmann D S, Becker C and Sengstock K 2012 *Nat. Phys.* **8** 813
- [17] Krauser J S, Ebling U, Fläschner N, Heinze J, Sengstock K, Lewenstein M, Eckardt A and Becker C 2014 *Science* **343** 157
- [18] Ebling U, Krauser J S, Fläschner N, Sengstock K, Becker C, Lewenstein M and Eckardt A 2014 *Phys. Rev. X* **4** 021011
- [19] Dong Y and Pu H 2013 *Phys. Rev. A* **87** 043610
- [20] Wei D, Xiong D Z, Chen H X and Zhang J 2007 *Chin. Phys. Lett.* **24** 679
- [21] Wei D, Xiong D Z, Chen H X, Wang P J, Guo L and Zhang J 2007 *Chin. Phys. Lett.* **24** 1541
- [22] Xiong D Z, Chen H X, Wang P J, Yu X D, Gao F and Zhang J 2008 *Chin. Phys. Lett.* **25** 843
- [23] Chai S J, Wang P J, Fu Z K, Huang L H and Zhang J 2012 *Acta Sin. Quantum Opt.* **18** 171
- [24] Huang L H, Meng Z M, Wang P J, Peng P, Zhang S L, Chen L C, Li D H, Zhou Q and Zhang J 2016 *Nat. Phys.* **12** 540